LAWRENCE
LIVERMORE
NATIONAL
LABORATORY

LLNL-JRNL-663317

Formation of ultra-relativistic electron rings from a laser wakefield accelerator

B. B. Pollock, F. Tsung, F. Albert, J. L. Shaw, C. E. Clayton, A. Davidson, N. Lemos, K. A. Marsh, A. Pak, J. E. Ralph, W. B. Mori, C. Joshi

October 28, 2014

Physical Review Letters

Disclaimer

Formation of ultra-relativistic electron rings from a laser wakefield accelerator

B. B. Pollock,[1,*] F. S. Tsung,[2] F. Albert,[1] J. L. Shaw,[2] C. E. Clayton,[2] A. Davidson,[2] N. Lemos,[2] K. A. Marsh,[2] A. Pak,[1] J. E. Ralph,[1] W. B. Mori,[2] C. Joshi[2]

[1] *Lawrence Livermore National Laboratory, 7000 East Ave., Livermore, CA 94550*
[2] *University of California, Los Angeles, 405 Hilgard Ave., Los Angeles, CA 90095*

(Date textdate; Received textdate; Revised textdate; Accepted textdate; Published textdate)

Ultra-relativistic-energy electron ring structures have been observed from laser wakefield acceleration experiments in the blowout regime. These electron rings had 100-300 MeV energies with 5-30% energy spread and 10's of pC of charge, and were observed over a wide parameter space in plasma density, length, and composition. 3-D PIC simulations show that laser intensity enhancement in the wake leads to sheath splitting and the formation of a hollow toroidal pocket in the electron density around the wake behind the first wake period. If the laser propagates over a distance greater than the ideal dephasing length, some of the dephasing electrons in the second period can become trapped within the pocket and form an ultra-relativistic ring of electrons that propagates in free space over a meter-scale distance upon exiting the plasma.

PACS numbers: 52.38.Kd, 41.75.Jv, 52.35.Mw

As conventional high-energy radio-frequency (RF) accelerators become large and extremely expensive, there is considerable interest in developing alternative methods for accelerating charged particles [1]. One such scheme that uses relativistic plasma waves produced by intense laser pulses is known as laser wakefield acceleration (LWFA) [2] and can accelerate particles orders of magnitude more rapidly than the current RF technology. The energy and reliability of LWFA-produced electron beams has steadily improved in the last decade [3–6] with continued advances in laser technology, plasma diagnostics, and modeling capabilities. As a result, the detailed physics of the wake and potential applications for the electron beams are being more thoroughly investigated than ever before.

In this Letter, we show through experiments that, under certain conditions, a LWFA can produce a highly-relativistic spatial ring of electrons in addition to the on-axis electron beam characteristic of this technique. Relativistic electron rings have been proposed in the literature as a driver for a two-beam accelerator [7] and for collective acceleration of trapped positive charges [8] in a conventional accelerator. The generation of such electron rings in this work is confirmed and explained using three-dimensional (3-D) particle-in-cell (PIC) code simulations, where the formation of the ring depends upon dynamic evolution of the driving laser pulse and the plasma wave. Furthermore, this ring structure propagates in free space as a relativistic potential well after exiting the plasma, making it attractive for trapping positively charged particles.

LWFA occurs when a short, relativistically-intense laser pulse is focused into a low-density gas or preformed underdense plasma. In order to access the so-called "blowout" regime [9], the pulse duration $c\tau$ must be shorter than one-half of the plasma period $\lambda_p = 2\pi c/\omega_p$, and the normalized vector potential of the laser $a_0 = eA/mc$ must satisfy $2 < a_0 < 2\omega_0/\omega_p$. Here, A is the laser vector potential, ω_0 is the laser angular frequency, and $\omega_p = \sqrt{n_e e^2/\epsilon_0 m_e}$ is the electron plasma frequency with n_e the electron density. Under these conditions, gas is readily ionized via tunnel ionization and plasma electrons at the front of the laser pulse are expelled from the laser axis by its transverse ponderomotive force. As a result of this near-complete expulsion of electrons, a region containing only the more massive ions, which are immobile on the short timescales of interest here (τ <100 fs), is formed near the laser axis. The laser continues to propagate through the plasma, and electrons behind the pulse are drawn back toward the laser axis by the space charge of the ions; these electrons overshoot the axis and set up the plasma wake. For sufficiently high laser power $P > P_c = (n_c/n_e)17GW$ and a matched laser spot size $w_0 = R_B = 2\sqrt{a_0}/k_p$[9], the laser pulse can be self-guided by this blown-out electron density profile at its focused spot size for extended distances, which allows the laser intensity to remain high enough to drive the plasma wake for 10's of Rayleigh lengths [10]. Here P_c is the critical power for relativistic self-focusing [11], n_c is the critical density for the laser wavelength, R_B is the maximum radius of the blown-out region ("bucket"), and $k_p = 2\pi/\lambda_p$ is the plasma wavenumber.

In the blowout regime, simulations indicate that the electron plasma wave induced by the laser pulse persists for 5-10 periods before phase mixing of the returning electrons causes a loss of coherence in the wake structure. Some of the electrons can become trapped not only in the first but also in the subsequent buckets and undergo acceleration. Simulations reveal that electrons trapped in the second bucket of a LWFA can eventually form a spatial ring structure as they interact with the dynamically-evolving first two buckets, where the evolution is due to laser self-focusing and dephasing of the electrons. In this Letter, we experimentally show the formation of ultra-

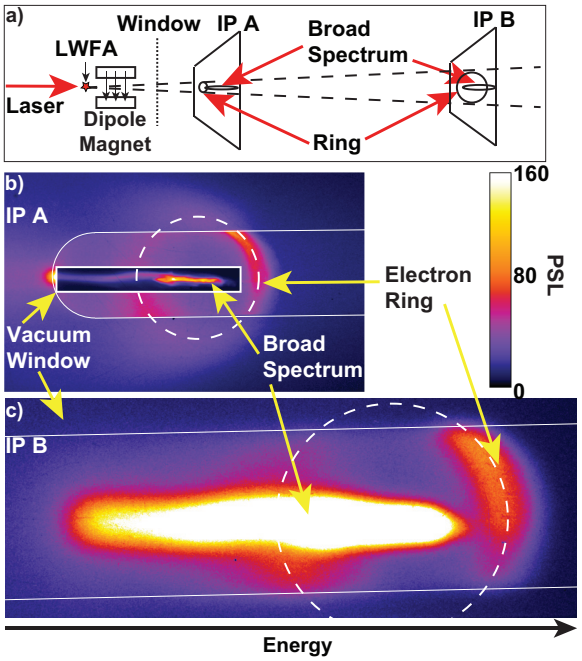

FIG. 1. a) Top view schematic of the electron spectrometer. Electrons are dispersed out of the page. Two image plates (IP) are used to record the electron flux exiting a vacuum window which is 12.5 cm (225 mrad) tall and 2.5 cm (45 mrad) wide with rounded top and bottom edges and consists of a 50 μm thick Al foil and a 65 μm thick mylar foil. IP A is located 62.2 cm from the plasma exit and IP B is located an additional 73.9 cm from IP A. b) False-color image of IP A electron data (after the dipole magnet) from a 10 mm gas cell filled with a mixture of 90/10% of He/N_2 (by partial pressure) and producing an electron density of 4.7×10^{18} cm^{-3} while driven by 50 TW of coupled laser power. Also shown on IP A is the shadow-projection of the vacuum window (outer, rounded rectangle), a dashed circle fitted to the peak-intensity portion of the visible ring structure, and a box-out (inner rectangle) that has been artificially attenuated by a factor of 10 from its surroundings to use the color bar (in photo-stimulated luminescence (PSL), which is proportional to the electron flux) on the right. Note: the vacuum window clipped a portion of the ring structure. c) False-color image of the same data as recorded on IP B. The features are more diffuse than on IP A due to electron scattering in IP A and the additional propagation in air. The direction of increasing energy (arrow at the bottom) applies only to the broadband spectrum. Each point on the ring structure has a different angle through the image plates and so exit angle and energy are still coupled (see text).

relativistic electron rings that are quasi-monoenergetic with $\Delta E/E$ of 5-30%, have expansion angles of ~50-100 mrad, and consist of 10-100 pC of charge. Rings are observed with LWFA operating in both the self- [12] and ionization-injection [13, 14] regimes of electron trapping when the plasma length is longer than the ideal dephasing length [9] so that the laser and the wake have each undergone significant transverse and longitudinal evolution. The particular example discussed in detail in this Letter utilizes ionization-induced injection.

The experiments are conducted at the Jupiter Laser Facility, Lawrence Livermore National Laboratory, using the Callisto Ti:Sapphire laser system. The laser beam, which nominally delivers 200 TW of power in a 60 fs laser pulse, is focused with an f/8, off-axis parabolic mirror to a 12 μm full-width at half-maximum (FWHM) spot (containing 50% of the laser power) at a position 500-750 μm inside a gas cell target. The gas cell length was varied between 6 and 10 mm (2-3 times the ideal dephasing length for the electron densities investigated here). The gas composition was varied from pure He to He/N_2 mixtures containing up to 10% N_2 by partial pressure. The entrance of the gas cell is a 500 μm diameter aperture, and the exit aperture is 1 mm in diameter to allow for uncoupled light from the f/8 beam to propagate out of the cell. For coupled laser powers of 30-60 TW, or a_0=2-2.8, the LWFA process evolves from the forced wakefield [15] into the blowout regime. In addition to the high-intensity pulse used to drive the wake, a 100 fs low-energy probe beam is utilized for transverse interferometric measurements of the plasma density through the transparent walls of the gas cell. We have previously shown measurements of the electron density and of the self-guiding and spectral shifting of the laser pulse under similar conditions [16] indicating that the laser pulse indeed propagates over an extended distance while forming a wake. After exiting the gas cell, electrons are dispersed by a 20 cm-long, 0.42 T dipole magnet, exit the vacuum chamber, and are recorded on two Fuji BAS-MS image plates (IP A and B) as shown in Fig. 1a to determine independently their energy and exit angle upon leaving the plasma [17, 18].

Under these laser and target conditions, the electron signal typically consists of an on-axis beam with a broad energy spectrum and a 1-5 mrad transverse beam divergence. In addition to this broadband signal, an electron ring is also observed in some cases, as seen in Figs. 1b and 1c. Since features of each electron signal are present on two successive image plates, the energy and the angle of exit from the plasma of each feature is independently determined following the analysis procedure described in [18]. By integrating the charge transversely along the dispersion direction in Figs. 1b and 1c, the spatial distribution of the electron signals on each image plate are compared to identify the common features. The equations of motion for an electron traveling from the plasma, through the known field-distribution of the magnetic dipole, and to the IPs are then solved in order to map a unique energy and plasma exit angle to the image plate locations of a particular feature. This analysis yields an exit angle of 41 mrad from the vacuum laser axis for electrons in the broadband feature shown in Figs. 1b and 1c. Using this non-zero exit angle, the resulting spectrum for this broadband beam is uniquely determined and is shown in Fig. 2a. Such a

continuous spectrum is consistent with previous observations of broadband spectra when using ionization injection because charge is continuously injected into the wake [4, 13, 16, 19]. Depending on the composition of the plasma, this broad feature can vary in its spectral peaks and maximum energy; however, the ring feature typically has an energy spread substantially smaller than that of the broadband feature.

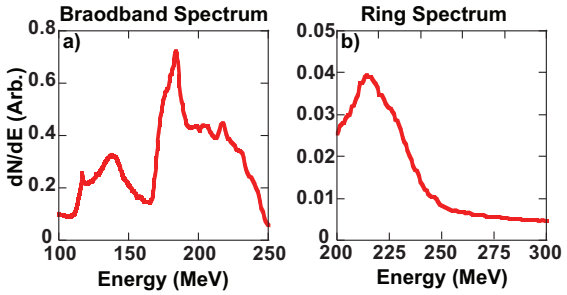

FIG. 2. Spectra for the a) broadband and b) ring electron features in Figs. 1b and 1c.

Applying the analysis procedure again to various positions around the ring reveals that all of the ring electrons have nearly the same energy of 215 MeV but each point around the ring has a different exit angle from the plasma. Electrons in the portion of the ring on the left side of Fig. 1b have an exit angle of 79 mrad; electrons on the opposite side (the "high-energy" side of the image plate) have only a 14 mrad exit angle (65 mrad full opening angle). Since each position on the ring has a different angle as it leaves the plasma, the correlation of energy and spatial position varies around the ring, and a simple energy axis cannot be assigned. The spectrum of the electrons with the 14 mrad exit angle is shown in Fig. 2b, and exhibits a 19% FWHM energy spread. In addition to the two-screen energy analysis, the shape of the ring also indicates that azimuthally the energy must be nearly constant. If the energy varied around the ring, then the ring would be elliptical after going through the magnet since the Larmor radius is energy dependent. Further, fitting a circle to this ring feature in both image plate planes yields a ∼65 mrad expansion from A to B, which is also consistent with assuming an initial point source for the ring at the plasma exit (as shown schematically in Fig. 1a) which expands in free space at 65 mrad. From this, we infer that a round ring of electrons with azimuthally-uniform energy was produced in the plasma, and in traversing the dipole magnet simply received a vertical shift to its trajectory from the $\mathbf{v} \times \mathbf{B}$ force. Over the course of the experiment, the ring peak energies varied from 135-280 MeV, with energy spreads of 5-30%, and the opening angles varied from 50-100 mrad.

In order to understand the ring formation physics, 3-D PIC simulations using the code OSIRIS [20] have been performed for an a_0=2.8, 65 fs, 800 nm, 15 μm diffraction-limited spot size (w_0) laser pulse propagating through 1 cm of plasma with an electron density of 3×10^{18} cm^{-3}. This simulation utilizes a moving window [21] and includes ADK [22] tunnel ionization of an initially-neutral mixture of 98% He and 2% N_2 gas. The dopant concentration is lower than in the example data described above, but, since diffraction-limited laser pulse simulations routinely show more trapped electrons than experiments with the same dopant concentration, it is often necessary to lower the dopant level in order to match experimental data. For an 800 nm laser, the simulation parameters are: c/ω_p = 1.46 μm; simulation box size = 800 x 1350 x 1350 c/ω_0 = 101.86 x 171.89 x 171.89 μm; grid = 4000 x 300 x 300; transverse resolution $k_p d_{x\perp}$=0.15; longitudinal resolution $k_0 d_{x\parallel}$=0.2; and 2 particles per cell per species.

Simulations of this experiment show that the ring formation is brought about by the electrons trapped in the second bucket interacting with the dynamically-evolving wake structure. The wake needs to evolve into the nonlinear blowout regime [9, 12], where the ponderomotive force of the laser (or space charge force of an intense particle beam) nearly expels all of the plasma electrons. These electrons form a narrow sheath; for laser drivers, this sheath is not as well defined and it splits. Although not shown here, the trajectories of electrons starting close to the axis cross those starting farther away from the axis. This splitting leads to the formation of toroidal pockets within the wake where relativistic electrons can be accelerated and guided off axis. The mechanism for how trapped electrons end up in these pockets is revealed in 3-D simulations of this experiment (simulations without the Nitrogen were also performed). In Fig. 3, we present 2-dimensional slices of the electron density and the laser pulse (3a, 3c, and 3e) and the corresponding contour maps of the wake focusing/defocusing force, $\mathbf{F}_\perp$=-e$(\mathbf{E} + \mathbf{v_z} \times \mathbf{B})_\perp$ (3b, 3d, and 3f), from the simulation at 5 mm, 7.5 mm, and 10 mm of laser propagation. As seen in Fig. 3a, at 5 mm, ionization of the inner-shell electrons of Nitrogen has produced ionization-trapped charge inside the fully-formed wake, which is largely made up of He (the wake also includes outer-shell N electrons). In the simulations, electrons arising from different ionization states of gases can be identified. The trapping condition for electrons born inside a non-evolving wake is [13] $\Delta\psi = -1+\sqrt{1+(p_{\perp f}/(m_e c))^2}/\gamma_\phi$, where $\psi \equiv \frac{e(\phi - v_\phi A_z)}{mc^2}$ is the normalized wake potential, $p_{\perp f}$is the transverse momentum at the time of trapping, and γ_ϕ is the relativistic factor of the wake moving with phase velocity v_ϕ. Electrons that have higher ionization potentials are born near the peak of the laser field (close to the laser axis, e.g. from N_{6+}) and therefore have the largest initial ψ, allowing them to be more readily trapped in the first bucket. For the parameters of this experiment, γ_ϕ is sufficiently large initially that the trap-

ping condition is essentially $\Delta\psi = -1$. Electrons that are born earlier in the laser pulse have a smaller initial ψ and, as they slip back to the edge of the first bucket, often do not satisfy the trapping condition. These electrons thus slip into the second bucket, where they have another chance to satisfy the trapping condition if the wake is evolving. The wake can evolve from a combination of the beam loading of the trapped electrons [23] and the ponderomotive force enhancement from self-focusing and photon deceleration of the laser [24]. Both of these effects cause the size (radius) of the first bucket to increase, which causes the location of the minimum of the wake potential to move backward with respect to the laser pulse causing the effective wake phase velocity to drop. The drop in phase velocity is progressively greater in each successive bucket [25]. Therefore, electrons that could not satisfy the trapping condition in the first bucket can be trapped in the latter buckets as seen in Fig. 3a.

The wake at this point is in a weakly nonlinear regime so that the toroidal pocket has not formed yet. The curvature in the wave fronts at this time is due to a combination of nonlinear frequency shifts [26, 27] as well as transverse forces on the particles inside the wake. Furthermore, as seen in Fig. 3a, a group of He electrons reside near the axis just behind the first bucket. By comparing simulations with and without (not shown) Nitrogen, it is clear that the formation of this line of electrons is due to the modification of the wake near the axis at the back of the first bucket from beam loading caused by the trapped inner-shell Nitrogen electrons. The line of electrons in the second bucket then modifies the transverse forces. As shown in Fig. 3b, this results in a region of defocusing force for relativistic electrons near the axis. Consequently, the trapped electrons within the second bucket begin to be pushed away from the axis as they move forward into this region.

As the laser propagates further, its intensity (and ponderomotive force) increases due to photon deceleration and self-focusing. In addition, the self-trapped charge in the first bucket also increases the bubble size. Therefore, by 7.5 mm, as seen in Fig. 3c, blowout and the splitting of the sheath has begun to occur, leading to the formation of the toroidal pocket. Note that the line of He electrons in the second bucket is no longer present. Self-trapped electrons at larger radius begin to be located inside the toroidal pocket. As seen in 3d, electrons inside the pocket and on axis are in regions of focusing (guiding) fields. Although not shown, the fields within the pocket are also accelerating the electrons.

After further propagation (10 mm), the laser intensity and the beam load in the first bucket increase. As seen in 3e, this leads to the sheath splitting mentioned earlier, while the length of the first bucket gets longer. The toroidal pocket increases in size and those electrons on axis that run into the back of the first bucket are defocused (see Fig. 3f). As a result, a clean ring of electrons is

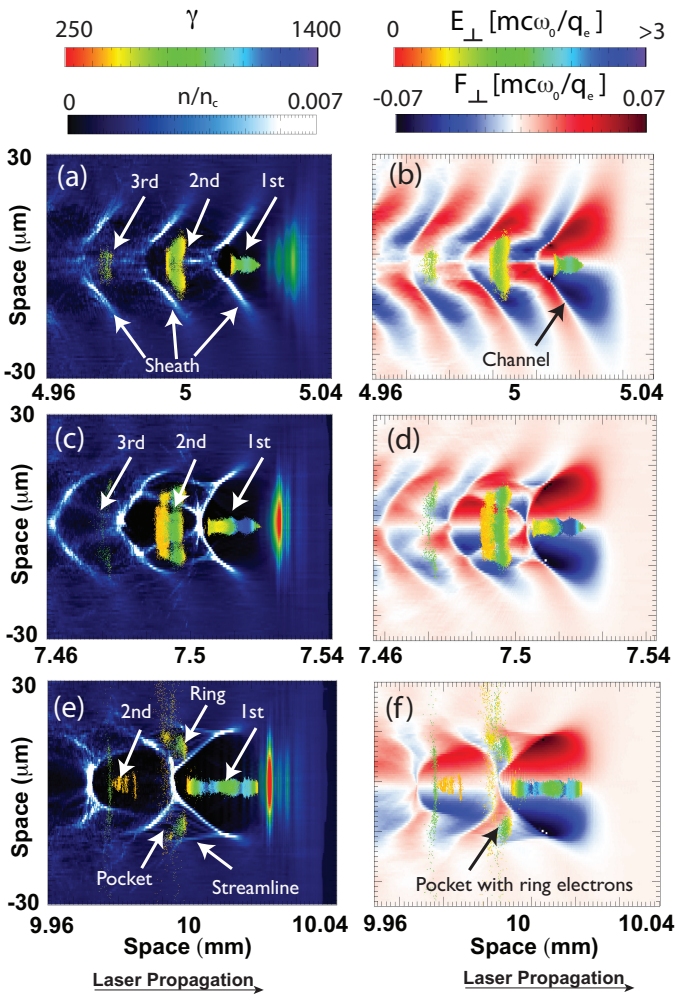

FIG. 3. a, c, e) Electron density maps from 3-D OSIRIS PIC simulations at 5, 7.5, and 10 mm of laser propagation, respectively. The $E_\perp$ color table corresponds to the envelope of the driving laser pulse at the right of the panels. b, d, f) Maps of the focusing force of the wake. White regions represent isocontours of zero focusing force. The key physical features are the electron sheath at the wake perimeter, the splitting of the electron sheath into an outer and inner streamline that results in the formation of a toroidal pocket as shown in e, and the electrons trapped into each of the first two buckets and the pocket.

formed, and they can stably propagate until they outrun the pocket.

Figure 4a shows the phase space of the N K-shell electrons from the second bucket, which exhibit three characteristic features. First, close to the axis are the remaining electrons toward the back of the second bucket that have large transverse momenta and relatively lower energies. Then, at a radius of 15 μm from the axis are the ring electrons, which have a smaller spread of transverse momenta. The characteristic divergence angle of the ring electrons can be found by taking the ratio of transverse to longitudinal momenta $P_r/P_z \approx 0.02$ (20 mrad), which

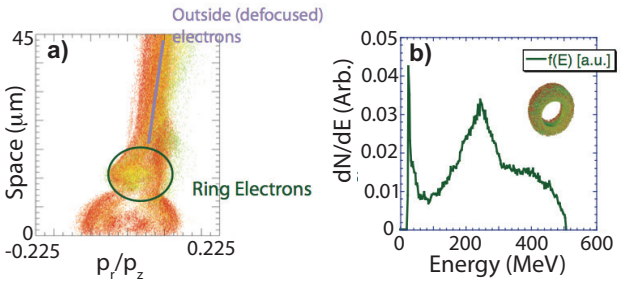

FIG. 4. a) Phase space plot of the electrons from the second bucket. b) Spectrum of electrons in the ring, with an inset showing the ring structure from the 3-D simulation.

is in reasonable agreement with the observed 30-35 mrad half-angle divergence in the experiment. Finally, at large radii are the electrons that are blown out by the expanding back of the first bucket.

The longitudinal spectrum of the electrons in the ring (see inset) is shown in Fig. 4b. Although the peak in the energy spectrum at 220 MeV is in reasonable agreement with the range of the experimental values, the energy spread is somewhat larger.

The process described here relies on the laser a_0 to increase sufficiently to split the electron sheath when electrons trapped in the second (or the third) bucket move (dephase) into a region in which the toroidal pocket is forming. Both self and ionization injection can occur in the second and third bucket when these structures are not in the blowout regime (but evolving). Lasers with unmatched spot sizes but with P/P_c significantly larger than unity can then evolve to matched spot sizes for which clear blowout and sheath crossing occurs over a wide range of parameters. Therefore, we believe the simulation shown here is valid over a wide range of plasma and laser conditions. Finally we note that, based on the mechanism described, it is also possible to conceive of other ways a ring could form, such as in a density down ramp. Here the ramp provides the wake elongation, although the laser evolution must still occur to produce the pockets.

We thank S. H. Glenzer and J. D. Moody for useful discussions of the data. We also acknowledge R. Cauble, S. Maricle, and J. Bonlie of the Callisto laser system. This work was performed under the auspices of the Department of Energy by the Lawrence Livermore National Laboratory and the University of California at Los Angeles under Contracts No. DE-AC52-07NA27344, No. DE-SC0008316, No. DE-SC0008491, and No. DE-NA0001833; NSF Grant No. ACI 1339893. This work was partially funded by the Laboratory Directed Research and Development Program under project tracking code 013-LW-076.

* electronic address: pollock6@llnl.gov

[1] *Laser Acceleration of Particles*, AIP Conference Proceedings **91**, Los Alamos, NM (1982), P. Channel ed.
[2] T. Tajima and J.M. Dawson, Phys Rev. Lett. **43**, 267 (1979).
[3] W.P. Leemans, B. Nagler, A.J. Gonsalves, Cs. Toth, K. Nakamura, C.G.R. Geddes, E. Esarey, C.B. Schroeder, and S.M. Hooker, Nature Phys. **2**, 696 (2006).
[4] C.E. Clayton et al., Phys. Rev. Lett. **105**, 105003 (2010).
[5] X. Wang et al., Nature Comm. **4**, 1988 (2013).
[6] H.T. Kim, K.H. Pae, H.J. Cha, I.J. Kim, T.J. Yu, J.H. Sung, S.K. Lee, T.M. Jeong, and J. Lee, Phys. Rev. Lett. **111**, 165002 (2013).
[7] G. Voss and T. Weiland, "The Wake Field Acceleration Mechanism," Deutsches Electronen-Synchrotron Internal Reports, DESY M82-10 (1982) and DESY 82-079 (1982), Hamburg, Germany.
[8] J.D. Lawson, Nature **218**, 430 (1968).
[9] W. Lu, M. Tzoufras, C. Joshi, F.S. Tsung, W.B. Mori, J. Vieira, R.A. Fonseca, and L.O. Silva, Phys. Rev. ST Accel. Beams **10**, 061301 (2007).
[10] J.E. Ralph, K.A. Marsh, A.E. Pak, W. Lu, C.E. Clayton, F. Fang, W.B. Mori, and C. Joshi, Phys. Rev. Lett. **102**, 175003 (2009).
[11] G.-Z. Sun, E. Ott, Y.C. Lee, and P. Guzdar, Phys. Fluids **30**, 526 (1987).
[12] W. Lu, C. Huang, M. Zhou, W.B. Mori, and T. Katsouleas, Phys. Rev. Lett. **96**, 165002 (2006).
[13] A. Pak, K.A. Marsh, S.F. Martins, W. Lu, W.B. Mori, and C. Joshi, Phys. Rev. Lett. **104**, 025003 (2010).
[14] C. McGuffey et al., Phys. Rev. Lett. **104**, 025004 (2010).
[15] V. Malka et al., Science **298**, 1596 (2002).
[16] B.B. Pollock et al., Phys. Rev. Lett. **107**, 045001 (2011).
[17] I. Blumenfeld et al., Nature **445**, 741 (2007).
[18] B.B. Pollock et al., in Proc. 2009 Particle Accel Conf., (Vancouver, Canada), pp. A14: 3035-3037, IEEE, 4-8 May 2009.
[19] F. Albert et al., Phys. Rev. Lett. **111**, 235004 (2013).
[20] R. Fonseca et al., Lect. Notes Comp. Sci. **2331**, 324 (2002).
[21] C. D. Decker, and W. B. Mori, Phys. Rev. Lett. **72**, 490 (1994).
[22] M.V. Ammosov, N.B. Delone, and V.P. Krainov, Sov. Phys. JETP **64**, 1191 (1986).
[23] M. Tzoufras, W. Lu, F. S. Tsung, C. Huang, W. B. Mori, T. Katsouleas, J. Vieira, R. A. Fonseca, and L. O. Silva, Phys. Rev. Lett. **101**, 145002 (2008).
[24] W.B. Mori, IEEE Journal of Quantum Elect. **33**, 1942 (1997).
[25] T. Katsouleas, Phys. Rev. A **33**, 2056 (1986).
[26] C. Joshi, W. B. Mori, T. Katsouleas, J. Dawson, J. M. Kindel, and D. W. Forslund, Nature **311**, 525 (1984).
[27] W. B. Mori, IEEE Trans. on Plasma Science, **PS – 15**, 88 (1987).